Electronic Supplementary Material (ESI) for Energy & Environmental Science.

Regulating electron spin orbital by sulfur atoms-doped Ti vacancies to manipulate spin flip for enhancing PEC water splitting

Yixuan Gao ‡[a,b], Min Zhang ‡[a], Qi Zhao ‡[a], Wen Liu ‡[b], Lirong Zheng [c], Jin Ouyang [d] and Na Na *[a]

---

a. *Key Laboratory of Radiopharmaceuticals, Ministry of Education, College of Chemistry, Beijing Normal University, Beijing, 100875, P.R. China, E-mail: nana@bnu.edu.cn*

b. *The Key Laboratory of Water and Sediment Sciences, Ministry of Education, College of Environmental Sciences and Engineering, Peking University, Beijing, 100871, P.R. China*

c. *Beijing Synchrotron Radiation Facility Institute of High Energy Physics Chinese Academy of Sciences, Beijing, 100049, P.R. China*

d. *Department of Chemistry, College of Arts and Sciences, Beijing Normal University at Zhuhai, Zhuhai, 519087, P.R. China*

‡ *These authors contributed equally to this work.*

Table of content

Section 1. Chemicals and Instrumentation

1.1 Chemicals

All chemicals were purchased from commercial sources and used without further purification. Tetrabutyl titanate was purchased from Macklin. Concentrated hydrochloric acid (HCl) was provided by Beijing Tongguang Fine Chemical Co., LTD. Sulfur powder was purchased from Aladdin. Thioacetamide (CH_3CSNH_2) was provided by Innochem. Carbon disulfide (CS_2) was purchased from Xiya Chemical Technology (Shandong) Co., LTD. High-purity water (18.2 MΩ·cm) supplied by Mill-Q Purification System. Fluorine-doped tin oxide (FTO) substrates (SnO_2: F, 15 $\Omega \cdot cm^{-2}$) were purchased from Wuhan Geao Instruments. Pretreatment was required before use. The FTO substrate was immersed in a solution of H_2O-ethanol-acetone mixed in equal proportions for ultrasonic cleaning for 20 min. Then cleaned with deionized (DI) water and dried in an oven at 40 ^oC for 15 min.

1.2 Instrumentation

The field emission scanning electron microscope (FESEM) (Model SU-8010, Japan) was adopted for imaging. The high-resolution transmission electron microscopy (HRTEM) of FEI Talos 200s TEM was applied for characterizations at an operating voltage of 200 kV. High-angle annular dark field scanning transmission electron microscopy (HAADF-STEM) measurements were taken on a transmission electron microscopy with a probe corrector (FEI Theims Z, Titan Cubed Themis G2300, JEM-ARM200F). Positron annihilation (PAL) of the samples were analyzed on a DPLS3000. X-ray diffraction measurement was characterized by Maxima XRD-7000 (Shimadzu, Japan). XPS spectra were recorded by using an X-ray spectrometer (Thermo ESCALAB 250 XI, PHI-5000 versaprobe III, Thermo Kalpha) with Al Kα excitation source. Raman spectra were recorded by Renishaw RM-1000 Raman spectrometer at room temperature, with 532 nm laser as excitation light source. The production of oxygen was detected by gas chromatography (GC, 2014C, Ar carrier, Shimadzu).

XAFS spectra at the Ti (4966 eV) K-edge were measured at the 1W1B beamline of the Beijing Synchrotron Radiation Facility (BSRF) and BL14W1 beamline of the Shanghai Synchrotron Radiation Facility (SSRF), respectively. The XANES spectra at the Ti L-edge and O K-edge were measured at National Synchrotron Radiation Laboratory (NSRL) in Hefei. The incident photon-to-current conversion efficiency (IPCE) was measured using a monochromator with a 300 W Xe light source (CEL-QPCE3000).

Section 2. Experimental methods

2.1 Synthesis of TiO_2 nanorods on FTO substrate

TiO_2 nanorods were grown on the conductive surface of FTO substrate by classical hydrothermal method. Add 6 mL concentrated HCl, 6 mL DI water and 200 μL tetrabutyl titanate into a 25 mL of Teflon-lined stainless steel autoclave and stir for 10 min to ensure uniformity. A treated piece of 1 cm×4.5 cm FTO was inserted diagonally into the Teflon-lined stainless steel autoclave with the conductive side down and heated at 170 ^oC for 10 h. After cooling to room temperature, the obtained white film on the FTO substate was washed with DI water and dried in an 40 ^oC oven.

2.2 Synthesis of Tiv-TiO_2 nanorods

The synthesized FTO coated with TiO_2 film was placed in a tubular furnace at 450 ^oC for 2 h. The inner cavity of a tubular furnace is in an air atmosphere.

2.3 Synthesis of S-Tiv-TiO_2 nanorods

The doping of S element was carried out in a tubular furnace in high-purity N_2 (99.999%). Specifically, a piece of FTO coated with Tiv-TiO_2 was placed onto a ceramic boat, and 15 mg sulfur powder was evenly dispersed on another ceramic boat, where the ceramic boat containing sulfur powder was placed upstream of the stream. The temperature of the tubular furnace was increased from room temperature to 250 ^oC at a rate of 3 ^oC/min and keep 2 h for the doping progress.

2.4 Synthesis of H_2S-Tiv-TiO_2 nanorods

H_2S-Tiv-TiO_2 was synthesized following the same procedure as S-Tiv-TiO_2, except for the addition of 50 mg thioacetamide and 1 mL DI water instead of 15 mg sulfur powder.

2.5 Synthesis of CS_2-Tiv-TiO_2 nanorods

The Tiv-TiO_2 and CS_2 were placed in a 25 mL Teflon-lined stainless steel autoclave and heated at 120 ^oC for 2 h.

Section 3. Detailed calculation procedures

3.1 carrier densities (N_d)

The charge carrier concentration (N_d) is obtained through the Mott-Schottky equation:

$$\frac{1}{C^2} = \frac{2}{q\varepsilon\varepsilon_0 N_d}(V - V_{FB} - \frac{kT}{Q})$$

Where C is the capacitance per unit area, q is the elementary charge, ε is the dielectric constant of TiO_2, ε_0 is the permittivity of vacuum, N_d is the charge carrier density, V is the electrode applied potential, k is the Boltzmann constant, and T is the absolute temperature. The N_d can be calculated as:

$$N_d = \frac{2}{q\varepsilon\varepsilon_0}\left[v\frac{d\left(\frac{1}{C^2}\right)}{d} \right]^{-1} N$$

3.2 The incident photon-to-current conversion efficiency (IPCE)

$$IPCE = \frac{1240 J_{photo}}{\lambda P}$$

Where J_{photo} is the measured photocurrent density, λ is the wavelength, P is the measured irradiance under monochromatic light.

3.3 The absorbed photon-to-current efficiency (APCE)

$$APCE = \frac{IPCE}{LHE}$$

The light harvesting efficiency (LHE, defined as the ratio of absorbed light to the incident light) of each photoanode is calculated from the UV-vis absorption spectra:

$$LHE = 1 - 10^{-A(\lambda)}$$

Where $A(\lambda)$ is the absorbance at wavelength λ.

3.4 The applied bias photon-to-current efficiency (ABPE)

$$ABPE = \frac{J_{photo}(1.23 - V_{app})}{P_{light}}$$

Where J_{photo} is the photocurrent density, V_{app} is the applied bias (V vs. RHE), P_{light} is the incident light density (100 mW·cm^{-2}).

3.5 Tauc plot equation

The bandgaps of the catalysts are confirmed via the equation:

$$(\alpha hv)^{1/n} = A(hv - E_g)$$

Where α is absorption coefficient, v light frequency, E_g is bandgap and A is a constant, n is 1/2 for direct bandgap semiconductor and 2 for the indirect bandgap semiconductor (rutile TiO_2 is direct bandgap semiconductor). The intercept of the extrapolated linear fit to the experimental data of a plot of $(\alpha hv)^{1/n}$-hv is the forbidden band width value (E_g).

Mott-Schottky plots were collected at 10 mV amplitude with a frequency of 500, 1000 and 2000 Hz. The flat band potential of TiO_2, S-Tiv-TiO_2, H_2S-Tiv-TiO_2 and CS_2-Tiv-TiO_2 are about -1.06, -1.15, -1.18 and -1.20 V vs. NHE, respectively. The flat band potential is ~0.10 V below the bottom of the conduction band for n-type semiconductors. The CB of TiO_2, S-Tiv-TiO_2, H_2S-Tiv-TiO_2 and CS_2-Tiv-TiO_2 are determined as -0.96, -1.05, -1.08 and -1.10 V vs. NHE, respectively.

Section 4. XAFS measurement and data analysis

The EXAFS spectra were obtained by subtracting the post-edge background from the overall absorption and then normalizing with respect to the edge-jump step. And then, the χ(k) data was Fourier transformed to real R-space to separate the EXAFS contributions from different coordination shells. In order to confirm the quantitative structural parameters around central atoms, least-squares curve parameter fitting was performed using the Artemis module. The following EXAFS equation was used for the calculation of the theoretical scattering amplitudes, phase shifts and the photoelectron mean free paths.

$$X(k)=\sum_j \frac{N_j S_O^2 F_j(k)}{kR_j^2}\exp\left[-2k^2\sigma_j^2\right]\exp\left[\frac{-2R_j}{\lambda(k)}\right]\sin\left[2kR_j+\Phi_j(k)\right]$$

R_j is the distance between the X-ray absorbing central atom and the atoms in the j^{th} atomic shell, N_j is the number of neighbors in the j^{th} atomic shell, S_0^2 is the amplitude reduction factor, $F_j(k)$ is the effective curved-wave backscattering amplitude, λ is the mean free path in Å, $\phi_j(k)$ is the phase shift (including the phase shift for each shell and the total central atom phase shift), σ_j is the Debye-Waller parameter of the j^{th} atomic shell (variation of distances around the average R_j). All fits were performed in the *R* space with k^2-weight for Ti K-edge.

Section 5. Electrochemical measurements

The PEC measurements were performed by electrochemical workstation (CH Instruments 660D). A 350 W xenon lamp (controlled by an external potentiostat) provided simulated solar light (100 mW·cm^{-2}) for the PEC tests. The electrolyte was 1 M NaOH (pH 14). Mott-Schottky plots of photocatalysts were carried out in N_2 purged 0.5 mol/L Na_2SO_4 electrolyte solutions. A typical three-electrode configuration was used with the catalysts (TiO_2, S-Tiv-TiO_2, H_2S-Tiv-TiO_2 and CS_2-Tiv-TiO_2) as the working electrode, a saturated $Hg/HgCl_2$ electrode as the reference electrode and a Pt foil (1×1 cm^2) as the counter electrode. According to the Nernst equation, the measured potentials vs. $Hg/HgCl_2$ were converted to the reversible hydrogen electrode (RHE) scale:

$$E_{RHE} = E_{Hg/HgCl_2} + 0.059\,pH + E^{\theta}_{Hg/HgCl_2}$$

Where $E^{\theta}_{Hg/HgCl_2}$= 0.24 V at 25 °C, E_{RHE} is the converted potential vs. RHE, $E_{Hg/HgCl_2}$ is the experimentally measured potential against the $Hg/HgCl_2$ reference.

Section 6. Computational methods and models

The density functional theory (DFT) calculations were performed using the Vienna ab initio Simulations Package (VASP, version 6.3.0). All geometry optimizations and self-consistent total-energy calculations were performed with the projector-augmented wave (PAW) method at the Perdew-Burke-Ernzerhof (PBE) densities functional level. The cut-off energy of 450 eV for plane-wave was set for all calculations while the atomic position was fully relaxed until the convergence criteria of force and energy was less than 0.02 eV/Å and 10^{-5} eV, respectively. The structural optimizations of TiO_2 (110) surface models were optimized with a 3×3×1 gamma-point centered k-point grid for Brillouin zone sampling and the top 3 atomic layers were allowed to fully relax while the bottom atomic 4 layer was fixed. Several defected and doped models were further built based on it. A vacuum slab exceeding 15 Å was employed in z direction so that interaction so that interaction between two neighboring surfaces can be neglected.

The OER performance was explored under the theoretical framework developed by Nørskov *et al*. The associative mechanism and a four-electron pathway were considered, according to which the OER elementary reactions are described as follows:

$$(1)\quad * + H_2O = *OH + H^+ + e^-$$

$$(2)\quad *OH = *O\cdot + H^+ + e^-$$

$$(3)\quad *O\cdot + H_2O = *OOH + H^+ + e^-$$

$$(4)\quad *OOH = * + O_2 + H^+ + e^-$$

Where * represents an active site. *OH, *O· and *OOH are the active sites with OH, O· and OOH intermediate adsorption, respectively. The free energy of the intermediates is defined as:

$$\Delta G = \Delta E + \Delta ZPE - T\Delta S$$

Where ΔE is the total energy change obtained from DFT calculations. ΔZPE and ΔS denote zero-point energy and entropy correction at room temperature (298.15 K), respectively. Since the equilibrium potential for OER is 1.23 V (vs. RHE), the full

energy of the four electrons transfer reaction is 4×1.23=4.92 eV. Therefore $^{\Delta G_4}$ was calculated by 4.92-$^{\Delta G_1}$-$^{\Delta G_2}$-$^{\Delta G_3}$ to avoid calculating the O_2 adsorption and desorption, which was known that DFT calculation could not accurately describe.

Section 7. Supplementary Figures and Tables

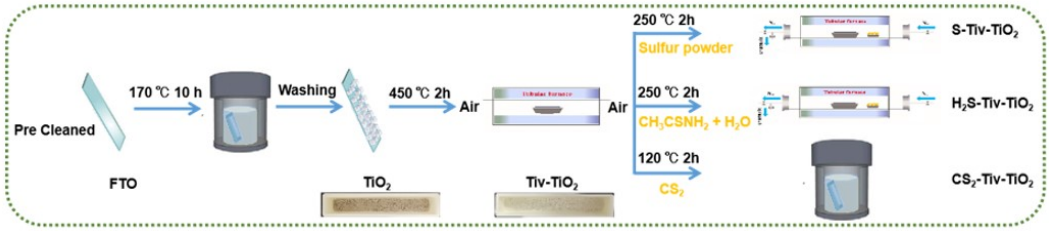

Fig. S1 Schematic representation of the preparation of sulfur-doped TiO_2 catalysts.

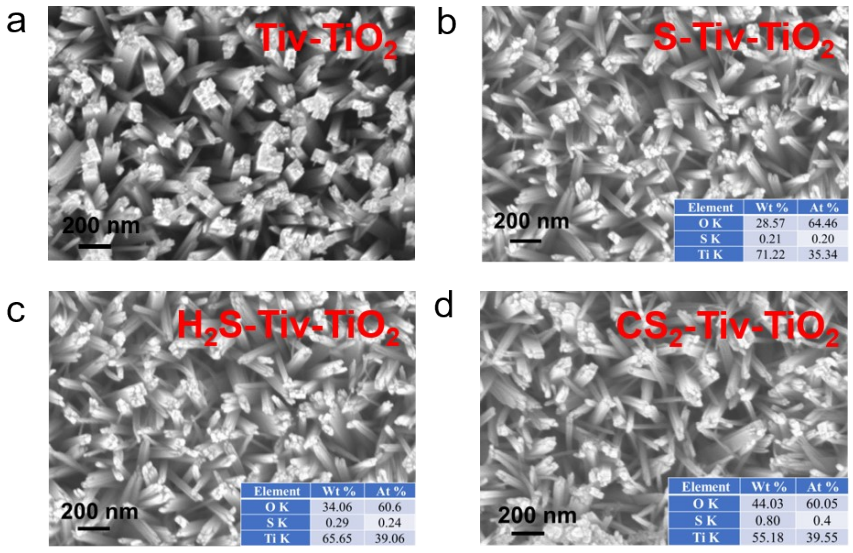

Fig. S2 SEM images of (a) Tiv-TiO_2, (b) S-Tiv-TiO_2, (c) H_2S-Tiv-TiO_2 and (d) CS_2-Tiv-TiO_2.

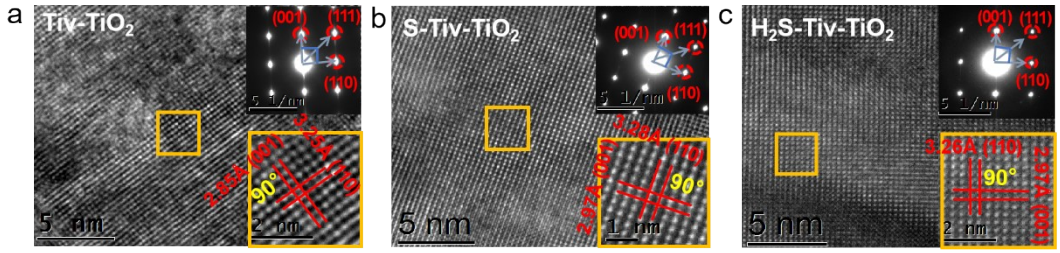

Fig. S3 HRTEM images of (a) Tiv-TiO_2, (b) S-Tiv-TiO_2 and (c) H_2S-Tiv-TiO_2 (inset: an enlarged HRTEM image of the selected area and the corresponding SAED patterns).

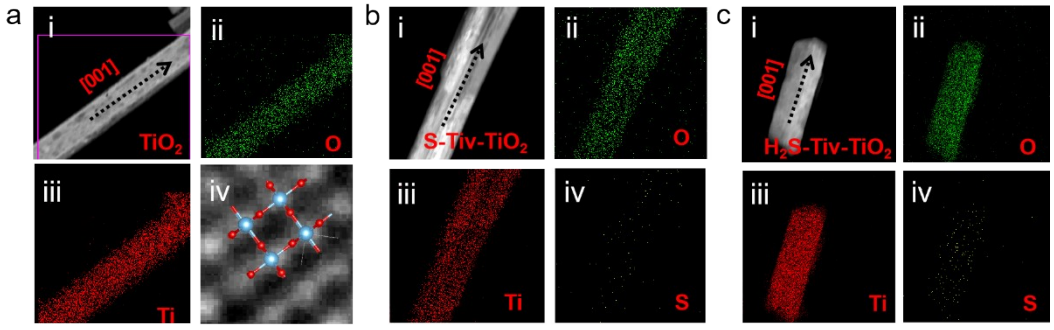

Fig. S4 EDS elemental mapping profiles of (a) TiO_2 and the enlarged of HRTEM (inset: the structure of TiO_2), (b) S-Tiv-TiO_2 and (c) H_2S-Tiv-TiO_2.

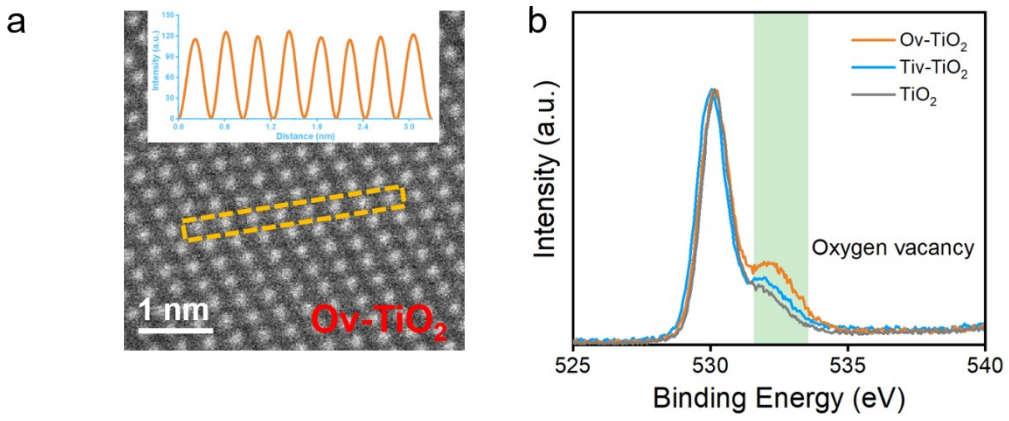

Fig. S5 (a) HAADF-STEM image of Ov-TiO_2 (inset: the corresponding intensity line profiles of the selected area). (b) XPS spectra of Ov-TiO_2, Tiv-TiO_2 and TiO_2.

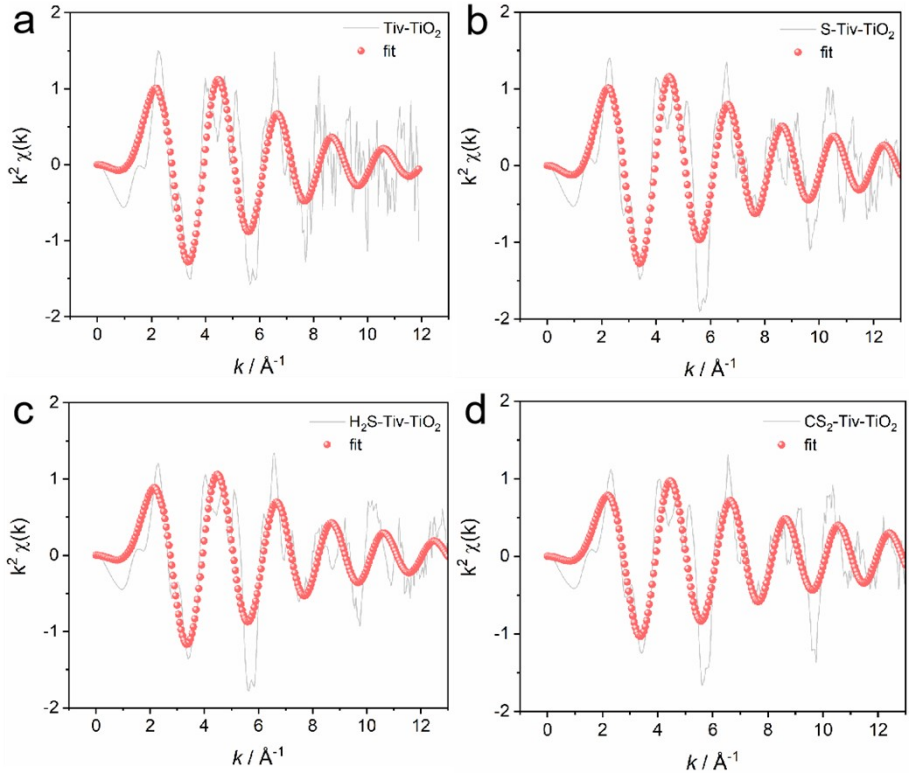

Fig. S6 Ti *K*-edge FT-EXAFS analysis of (a) Tiv-TiO_2, (b) S-Tiv-TiO_2, (c) H_2S-Tiv-TiO_2 and (d) CS_2-Tiv-TiO_2 in *k* space.

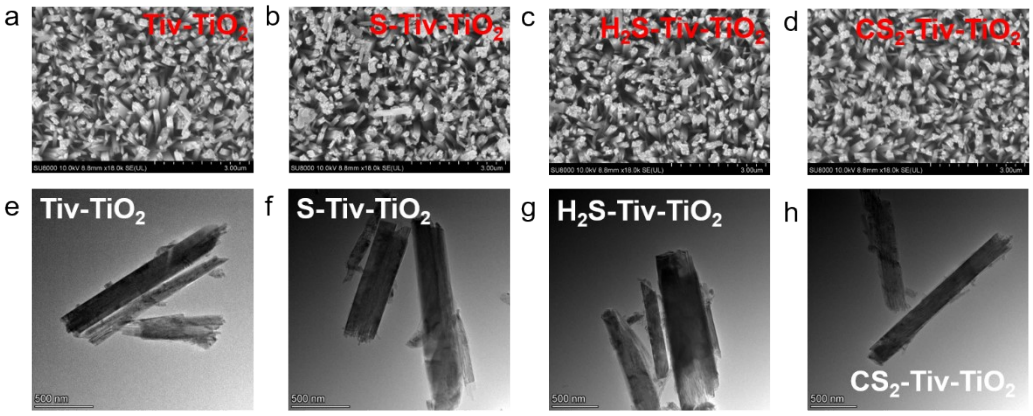

Fig. S7 SEM images of (a) Tiv-TiO_2, (b) S-Tiv-TiO_2, (c) H_2S-Tiv-TiO_2 and (d) CS_2-Tiv-TiO_2 after OER test. TEM images of (e) Tiv-TiO_2, (f) S-Tiv-TiO_2, (g) H_2S-Tiv-TiO_2 and (h) CS_2-Tiv-TiO_2 after OER test.

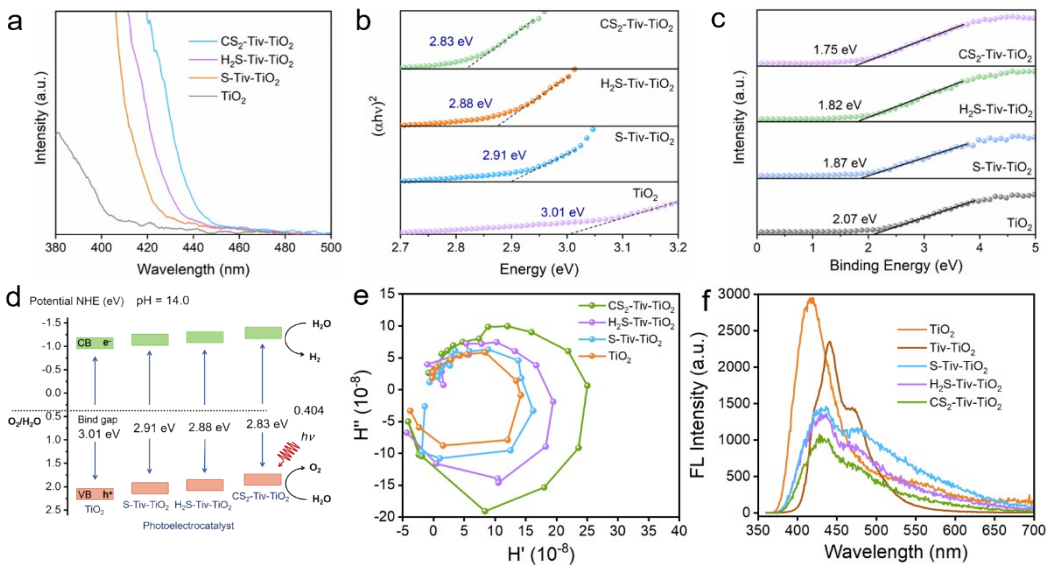

Fig. S8 (a) UV-vis absorption spectra and (b) Valence band obtained from XPS data for the catalysts. (c) Tauc plot analysis of the optical bandgaps derived from UV-vis spectra. (d) Schematic illustration of the relationship between VB and conduction band (CB), with bandgap marked. (e)

IMPS spectra of TiO_2, S-Tiv-TiO_2, H_2S-Tiv-TiO_2 and CS_2-Tiv-TiO_2. (f) Room-temperature PL emission spectra.

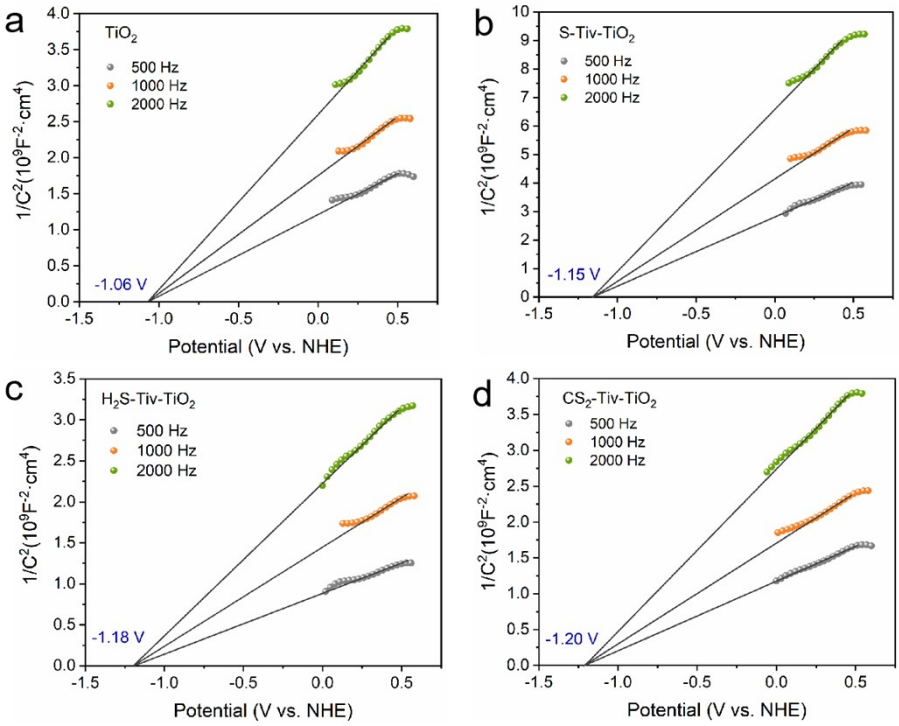

Fig. S9 Mott-Schottky plots under different frequencies for (a) TiO_2, (b) S-Tiv-TiO_2, (c) H_2S-Tiv-TiO_2 and (d) CS_2-Tiv-TiO_2.

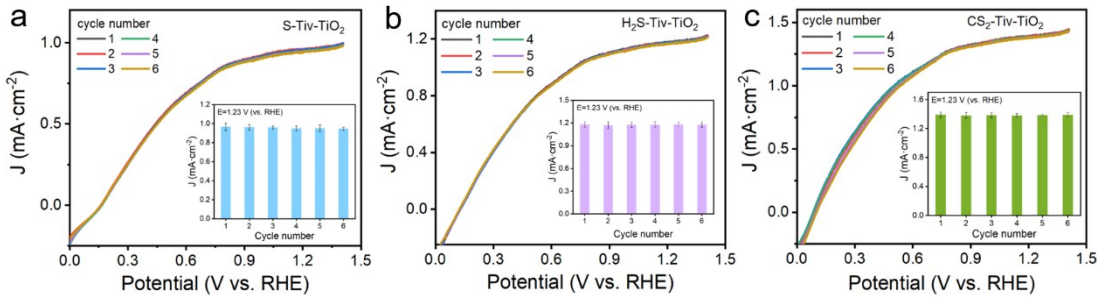

Fig. S10 Linear sweep voltammetry (LSV) curves of (a) S-Tiv-TiO_2, (b) H_2S-Tiv-TiO_2, (c) CS_2-Tiv-TiO_2 for 6 cycles (inset: the photocurrent values corresponding to 1.23V vs. RHE from LSV curves).

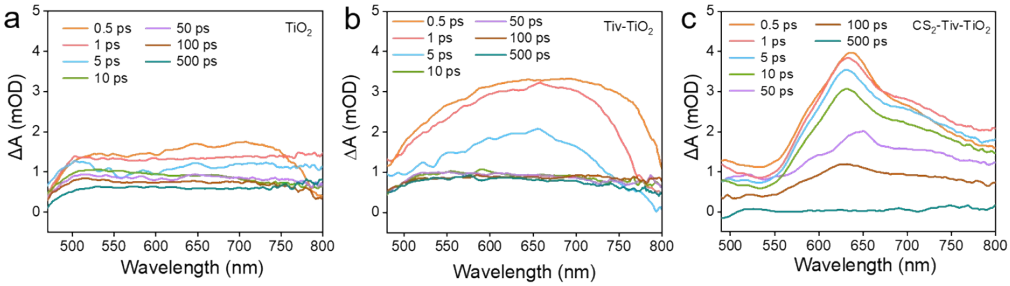

Fig. S11 The transient absorption spectra of (a) TiO_2, (b) Tiv-TiO_2, (c) CS_2-Tiv-TiO_2 observed in visible light region under 355 nm pump laser excitation.

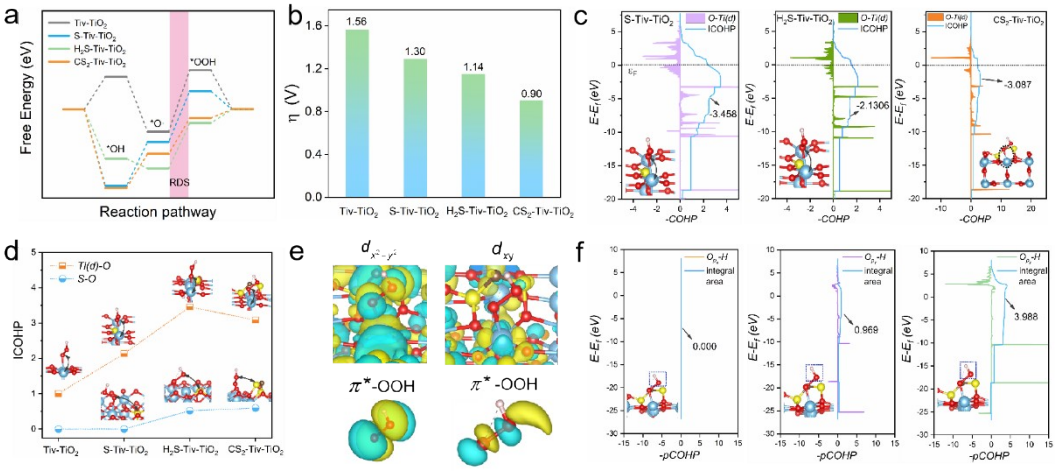

Fig. S12 (a) Gibbs free energy diagram for the four steps of OER and (b) the theoretical overpotential for Tiv-TiO_2, S-Tiv-TiO_2, H_2S-Tiv-TiO_2 and CS_2-Tiv-TiO_2. (c) COHP of the Ti-O pair and corresponding ICOHP of S-Tiv-TiO_2, H_2S-Tiv-TiO_2 and CS_2-Tiv-TiO_2, (d) The ICOHP of Ti-O and S-O pair for Tiv-TiO_2, S-Tiv-TiO_2, H_2S-Tiv-TiO_2 and CS_2-Tiv-TiO_2. (e) The wave functions between $d_{x^2-y^2}$ and d_{xy} orbitals and π^* orbitals are displayed along with their respective

energy levels. (f) Projected COHP of the H 1*s* and p_x, p_y, p_z orbitals of O and corresponding ICOHP of CS_2-Tiv-TiO_2.

Table S1. EXAFS fitting parameters at the Ti *K*-edge various samples.

Sample	CN	E_0	ΔR	σ^2
Tiv-TiO_2	5.4	-2.8	0.01	0.001
S-Tiv-TiO_2	5.6	-1.59	0.03	0.002
H_2S-Tiv-TiO_2	5.5	-4.07	0.01	0.003
CS_2-Tiv-TiO_2	5.6	-2.8	0.01	0.001

S_0^2 were set as 0.8 for all samples, according to the experimental EXAFS fit of Ti foil by fixing CN as known crystallographic value.
S_0^2 is the amplitude reduction factor; CN, coordination number; R, distance between absorber and backscatter atoms; σ^2, Debye-Waller factor to account for both thermal and structural disorders; ΔE_0, inner potential correction; R factor indicates the goodness of the fitting.

Table S2. The slope of Mott-Schottky curves and corresponding N_d for all catalysts.

Sample	Slope	N_d
Tiv-TiO_2	3.584×10^9	1.687×10^{17}
S-Tiv-TiO_2	1.797×10^9	3.365×10^{17}
H_2S-Tiv-TiO_2	1.494×10^9	4.047×10^{17}
CS_2-Tiv-TiO_2	1.2×10^9	5.039×10^{17}

Table S3. Amount of O_2 evolution for the samples during 6 hours and the corresponding rate of O_2 production.

Sample	Amount of O_2 during 6h ($\mu mol\cdot cm^{-2}$)	Oxygen production rate ($\mu mol\cdot cm^{-2}\cdot h^{-1}$)
Tiv-TiO_2	10.75	1.80
S-Tiv-TiO_2	26.45	4.45

H_2S-Tiv-TiO_2	48.41	8.11
CS_2-Tiv-TiO_2	73.17	12.19